2019

Metal-Organic Frameworks with Metal Catecholates for O2/N2 Separation

Samuel J. Stoneburner

Hakan Demir

WooSeok Jeong

Debmalya Ray

Xuan Zhang

See next page for additional authors

Authors

Samuel J. Stoneburner, Hakan Demir, WooSeok Jeong, Debmalya Ray, Xuan Zhang, Omar K. Farha, Christopher J. Cramer, Ilja Siepmann, and Laura Gagliardi

Metal-Organic Frameworks with Metal Catecholates for O_2/N_2 Separation

Hakan Demir,[a] Samuel J. Stoneburner,[a] WooSeok Jeong,[a] Debmalya Ray,[a] Xuan Zhang,[b] Omar K. Farha,[b] Christopher J. Cramer,[a] J. Ilja Siepmann,[a,c]* and Laura Gagliardi[a]*

[a] Department of Chemistry, Minnesota Supercomputing Institute, and Chemical Theory Center, University of Minnesota, 207 Pleasant Street Southeast, Minneapolis, MN 55455-0431, United States.

[b] Department of Chemistry, Northwestern University, 2145 Sheridan Road, Evanston, IL 60208, United States.

[c] Department of Chemical Engineering and Materials Science, University of Minnesota, 421 Washington Avenue SE, Minneapolis, MN 55455-0431, United States.

Abstract

Oxygen and nitrogen are widely produced feedstocks with diverse fields of applications, but are primarily obtained via the energy-intensive cryogenic distillation of air. More energy-efficient processes are desirable, and materials such as zeolites and metal-organic frameworks (MOFs) have been studied for air separation. Inspired by recent theoretical work identifying metal-catecholates for enhancement of O_2 selectivity MOFs, in this work the computation-ready experimental (CoRE) database of MOF structures was screened to identify promising candidates for incorporation of metal catecholates. Based on structural requirements, preliminary Grand-Canonical Monte Carlo simulations, and further constraints to ensure the computational feasibility, over 5,000 structures were eliminated and four MOFs (UiO-66(Zr), Ce-UiO-66, MOF-5, and IRMOF-14) were treated with periodic density functional theory (DFT). Metal catecholates (Mg, Co, Ni, Zn, and Cd) were selected based on cluster DFT calculations and were added to the shortlisted MOFs. Periodic DFT was used to compute O_2 and N_2 binding energies near metal catecholates. We find that the binding energies are primarily dependent on the metals in the metal catecholates, all of which bind O_2 quite strongly (80-258 kJ/mol) and have weaker binding for N_2 (3-148 kJ/mol). Of those studied here, Cd-catecholated MOFs are identified as the most promising.

Introduction

The production of oxygen gas is at enormous levels (>100 million tons/year) and oxygen gas is one of the most essential chemicals due to its various uses in medicine, chemical manufacturing, coal gasification, wastewater treatment, fuel cells, and the paper industry.[1–3] High-purity oxygen (>99%) is crucial for a variety of areas, such as medical,[3] military and aerospace,[4] semiconductor,[5] cylinder filling,[6] ozone generation,[6] plasma chemistry,[6] and oxy-fuel combustion[7] applications. For instance, for surgeries in the U.S., the minimum oxygen purity is 99%, and it is even higher in Japan (99.6%).[4] In semiconductor, military, and aerospace applications similar concentrations of 99.8%, 99.5%, and 99.5%, respectively, are required.[4] Thus, effective separation of oxygen and nitrogen from air can provide large sources of commodity gas that would lower the cost of the aforementioned applications.

Separation of O_2 and N_2 has been regarded as one of the most challenging separations due to their similar molecular sizes.[8] Cryogenic distillation has been used to produce O_2 at industrial scales since the 1920s.[9] However, the boiling points of O_2 and N_2 at 1 atm are -183 and -196 °C, respectively, and so a great deal of energy is required to condense the gases at very low temperatures.[10] Although cryogenic distillation is a proven technology for large quantities of air separation (>200 tons/day), for small and medium scale production more economical alternatives around room temperature such as membrane separation, vacuum and pressure swing adsorption (VSA, PSA) are possible.[11–13] It has been demonstrated that the PSA technique with current materials can provide oxygen at concentrations up to 95% for small and medium scale needs with much less energy than required for cryogenic distillation.[4,10]

Zeolites are traditionally used as adsorbents for many applications, including O_2/N_2 separation. Many zeolites have shown preference for N_2 over O_2 such as 4A, 5A, LiAgX, LiLSX, and Linde 10X zeolite, which are molecular sieves hosting different pore aperture sizes with disparate chemical contents in terms of silica amount and the absence/presence of various cations (Li, Ag).[14,15] The more favorable interactions for N_2 compared to O_2 have been suggested to arise from the potent interaction of the quadrupole moment of N_2 (-1.4 Debye.Å for N_2 vs. -0.4 Debye.Å for O_2)[16,17] with the electric field in the framework.[15,18] For obtaining O_2 with air separation, however, the adsorbent should selectively capture O_2 over N_2 around room temperature. Capturing O_2 would bring great economic benefit compared to zeolites since capturing lean gas with porous materials means smaller volumes of gas need to be processed. Metal-organic frameworks (MOFs)[19–22] are promising candidates for selective O_2 adsorption. MOFs can be efficient O_2 selective materials since they have much wider chemical diversity than traditional adsorbents as well as highly porous and functionalizable structures.

The basic concept underlying the construction of the MOFs is the linking of two building blocks, metal nodes and organic linkers, and so almost infinitely many MOFs can be constructed by combining different building blocks.[23] Recently, the number of experimental and theoretical MOFs has risen swiftly and several collections of structures involving MOFs such as the Cambridge Structural Database (CSD)[24], hypothetical MOFs (hMOFs)[23], computation-ready experimental MOFs (CoRE MOFs[25]), and ToBaCCo[26] have been reported.

Although high numbers of MOFs might initially appear to be an advantage, performance testing each MOF experimentally would be daunting in terms of time and financial resources. Computational tools can be highly beneficial in accelerating the experimental efforts to find the best material for a particular application. Grand-Canonical Monte Carlo (GCMC) is a molecular simulation method routinely used to investigate the adsorption thermodynamics in nanoporous materials having a wide range of structural diversity.[27–29] For instance, Moghadam et al.[30] performed GCMC simulations for more than 2900 MOFs in the CoRE MOF database to acquire adsorption loadings and deliverable O_2 capacity, both at 298 K. Having identified top MOFs from GCMC simulations, they synthesized UMCM-152 and achieved the highest deliverable oxygen capacity (22.5% higher than the second top material in the literature) and matching loadings with those in experimental isotherms. DeCoste et al.[31] made a similar analysis for 10,000 MOFs and identified NU-125 as a better O_2 storage material than NaX and Norit activated carbon (237%, and 98%, respectively) in terms of excess capacity. GCMC simulations can be categorized into two types: force-field based and ab-initio based simulations. The accuracy of the former heavily relies on the force field parameters which determine the intramolecular/intermolecular interactions.[32] Many examples have been demonstrated where generic force fields can make predictions close to experimental adsorption values for sorbates such as CH_4 and H_2.[33–35] However, when Zeitler et al.[36] studied 98 materials for O_2 adsorption using a generic force field, UFF,[37] their comparisons with experimental data demonstrated that UFF is incapable of describing O_2-open metal site interactions accurately. Density functional theory (DFT) is a relatively affordable quantum chemical method which can be used to derive specialized force fields that could significantly improve generic force field predictions and reproduce experimental data,[38–40] but the use of DFT-based force fields is generally limited to the specific systems for which they were designed. Besides, DFT can be used to study adsorption in systems for which a force field is unavailable.[41] Wang et al.[42] studied O_2 adsorption in $M_3(BTC)_2$ (M= Cr, Mn, Fe, Co, Ni and Cu) with PBE-D2 and found $Ni_3(BTC)_2$ to be a potentially useful oxygen adsorbent that could favorably bind O_2 over N_2. Parkes et al.[43] screened the binding energy of O_2 and N_2 in M_2(dobdc) and $M_3(BTC)_2$ with 14 different metals with PBE-D2. The MOFs substituted with early transition metals were recommended as the best materials for selectively capturing O_2 over N_2 because both MOFs show higher O_2 binding energy with early transition metals than with late transition metals. Similar studies have been conducted by Gallis et al.[44], Verma et al.[45] and Xiao et al.[46] on M-BTC (M = Mn, Fe, Co, Cu), Fe_2(dobdc), and Co-BTTri and Co-BDTriP, respectively.

Open-metal MOFs that have been synthesized and studied experimentally regarding O_2 adsorption/separation typically have had critical performance failures such as poor cyclability and/or limited separation performance except at relatively low temperatures. For example, $Cr_3(BTC)_2$ exhibits much more favorable O_2 adsorption interaction compared to the physisorption of N_2, driven by a partial electron transfer from Cr^{2+} to the bound O_2 sorbate, but it shows a steady decrease in O_2 uptake for repeated cycles.[47] A Co(II) carborane-based MOF shows an O_2/N_2 selectivity of 6.5 at low pressure, but it quickly diminishes to ~2 at higher pressures.[48] Bloch et al.[1] have demonstrated that Fe_2(dobdc) is an O_2 selective MOF, but with irreversible O_2 binding above 226 K. They found that charge transfer from Fe(II) to O_2 changes from partial transfer at low temperature into complete transfer at room temperature. Later, Bloch et al.[49] reported that Cr-BTT exhibits rapid O_2 adsorption/desorption kinetics with good O_2/N_2 selectivity. These studies

illustrated the importance of the presence of redox-active metal in MOFs for preferential O_2 uptake over N_2. However, these open metal MOFs have been known to lose crystallinity and O_2 adsorption performance when adsorption conditions are not well controlled.[50] In contrast, Co-BTTri and Co-BDTriP showed good recyclability up to 10 cycles, but they exhibited high selectivities only at low temperatures (13 and 40 at 243 K for Co-BTTri and Co-BDTriP, respectively).[50] Low O_2/N_2 selectivity at room temperature is a common problem for MOFs. For example, it has been shown that MOF-177 possesses an O_2/N_2 selectivity of 1.8 at 298 K, 1 atm.[51] Likewise, UMCM-1 exhibits an O_2/N_2 selectivity of 1.64 at similar conditions (298 K, 0.96 bar).[52] MOFs demonstrating high O_2/N_2 selectivity around room temperature have not been reported yet to the best of our knowledge, which is a gap in material space that is one of the motives of this work.

Metalated catecholate linkers have brought new opportunities in adsorption due to the strong interactions between the open metal site in the metal catecholate with multiple sorbates (e.g., Weston et al.[53]), and thus could be used to obtain higher O_2/N_2 selectivity and O_2 uptake. A previous computational investigation[54] predicted that metal catecholates (Mg, Sc, Ti, V, Cr, Mn, Fe, Co, Ni, Cu, and Zn) could be beneficial for air separation. Except for Cu catecholate, all metal catecholates were shown to interact stronger with O_2 than N_2. Fe and Zn catecholates were suggested as the most appropriate choices due to relatively weak affinity towards O_2, which is expected to result in a relatively easy desorption and improve the regenerability of the system. In addition, generation of strong adsorption sites at the metal-catecholate rather than at nodes could be a good way to avoid structural stability issues. Conventional open metal sites in metal nodes are closely related to structural integrity, since the weakest bond in MOFs is the metal-ligand bond.[55,56] In contrast, the metal sites in metalated catecholate linkers are not directly bonded to the pristine MOF structure and are not expected to play a significant role in the general structural stability. While there are additional synthetic and reusability challenges that arise from the reactivity of the catecholates and the undercoordination of the metal, metal-catecholates and related moieties have already been synthesized in several MOFs[57–61] and porous organic polymers[53,62–64], with applications in gas separations[62], gas storage[53], and catalysis[57,58,60,63,64]. For example, Fei et al.[58] reported the synthesis of UiO-66(Zr) with Cr-catecholates for oxidation catalysis with no loss of Cr and with good stability with respect to temperature and aqueous solvent. Similarly, Huang et al.[60] reported the synthesis of and hydroboration of carbonyls on ANL1-Ti$(OiPr)_2$ with no significant loss of the alkoxide-supported Ti, and Tanabe et al.[63] found that functionalizing a porous organic polymer with a Ta^V trialkyl resulted in no loss of thermal and structural robustness.

In this study, we aim to develop highly O_2 selective MOFs for O_2/N_2 separation by inserting metal-catecholates into experimentally known MOF structures. Our objective can be divided into two targets: to find parent MOF structures that can be good platforms for metalated structures, and then to develop metalated MOF structures from the parent ones. The scheme of this multi-stage work is depicted below in Figure 1. In the first stage several structural criteria, which are indicated in the Computational Methods section, are applied to CoRE MOFs to identify MOFs with appropriate pore space where metal catecholates could be incorporated. In the second stage the shortlisted MOFs are used, without any modification, in binary GCMC simulations (O_2/N_2 = 20:80) to predict O_2/N_2 selectivity at 1 bar, 298 K. MOFs with O_2/N_2 selectivity larger than 1 are considered to have

good potential for selective O_2 separation, inasmuch as they are not N_2-selective and will therefore not have structural effects counterproductive to our goal of O_2 selectivity. In the third stage metal-catecholate functionalized MOF structures are generated for the screened pristine MOFs, with the metals selected based on previous work[54] and new cluster DFT calculations. Duplicate metalation sites are excluded using an in-house developed code in Python. In the last stage a subset of the metalated MOF structures are chosen based on computational feasibility of structural optimization and the binding energies of O_2 and N_2 are calculated with periodic DFT.

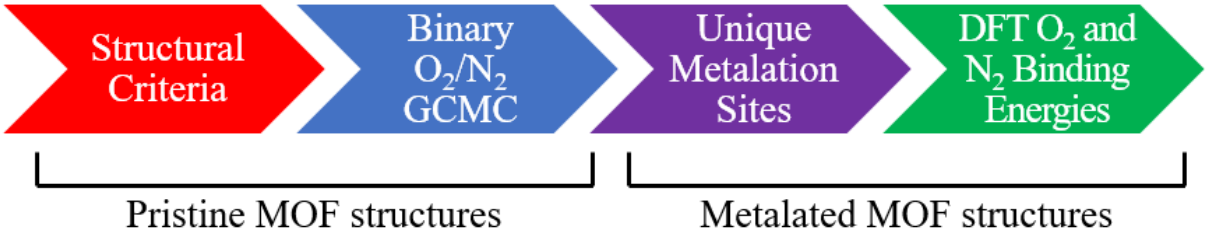

Figure 1. Multi-stage screening approach.

Computational Methods

Overview of the screening procedure

Our work consisted of multiple steps, summarized in Figure 2. The CoRE MOF database includes 5,109 experimentally reported MOF structures. The initial 5,109 structures were reduced to 2,867 by requiring 6-membered rings consisting of C and/or N atoms and requiring that at least two adjacent ring atoms have one H atom attached to each. These requirements ensured that the given structures have site(s) for inserting metalated catecholates, resulting in the selection of MOFs that have organic ligands containing benzene(-like) moiety such as 1,4-benzenedicarboxylate (BDC) and benzene-1,3,5-tricarboxylate (BTC).

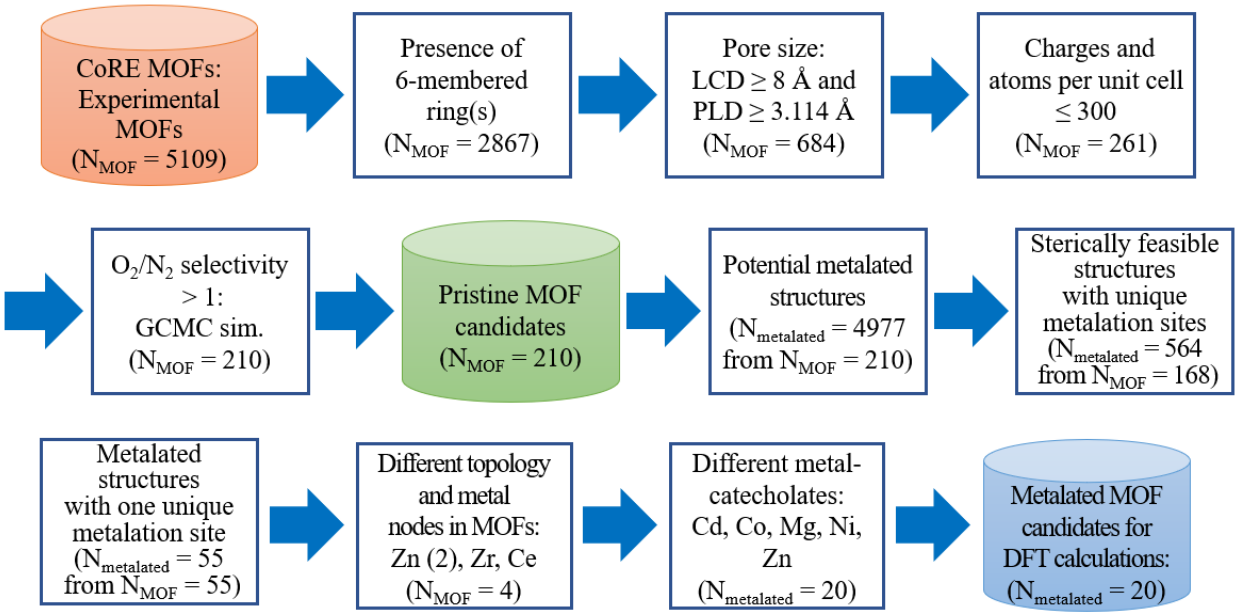

Figure 2. Screening process for selecting metalated MOF structures for DFT calculations.

Next, MOFs were required to have pore limiting diameters (PLD) larger than or equal to 3.114 Å and largest cavity diameters (LCD) larger than or equal to 8.000 Å. The pore limiting diameter (i.e., pore aperture diameter) minimum was chosen as 90% of the O_2 kinetic diameter, which filtered out most of the MOFs that would experience high diffusional constraints. The largest cavity diameter (i.e., largest pore diameter) was chosen so that there would be enough space available in the pore space to incorporate a metal catecholate. The pore specifications reduced the number of MOF structures to 684.

In anticipation of GCMC calculations and recognizing the need for relatively reliable charges for the framework atoms, MOFs were omitted that involve atoms for which there were not sufficient electron affinity and ionization potential data in the EQeq code,[65] mostly lanthanides and actinides. To reduce computational cost for subsequent periodic DFT calculations, MOFs were also required to have less than or equal to 300 atoms per unit cell. Thus, 261 MOF structures out of the original 5,109 survived to GCMC calculations. Note that omissions for computational feasibility took place only after the structural screening was complete, and so only 423 structures (i.e., less than 8.3% of the original 5,109) were excluded from GCMC calculations for the technical reasons described here. See the Supporting Information for further details on the size-excluded structures.

Structural Analysis

MOF structures were obtained from the CoRE MOF database, which includes experimentally reported structures only.[25] Potential sites for metal-catecholates, i.e., 6-membered rings of carbon and/or nitrogen atoms, of which two adjacent ring atoms have one H atom each attached, were identified using the geometry analysis tools of Platon.[66,67] Geometrical analysis on pore sizes and the number of open metal MOFs was conducted with Zeo++.[68] Additional structural analysis for

metalated MOF structures was performed with custom in-house code as described in subsequent sections.

GCMC

Binary GCMC simulations for binary gas mixtures (20% O_2, 80% N_2) were carried out using the RASPA[69] code to obtain O_2 and N_2 loadings and O_2/N_2 selectivity data at p = 1 bar and T = 298 K as follows

$$S_{O_2/N_2} = \frac{N_{O_2}/N_{N_2}}{x_{O_2}/x_{N_2}} \quad (1)$$

where N is the gas uptake (in units of molecules per simulation cell) and x is the mole fraction of this component in the feed mixture. Adsorbate-adsorbate and adsorbate-MOF interactions were modeled through a combination of Lennard-Jones and Coulomb potentials. The force field parameters for O_2[70]and N_2[16] (3-site models) were obtained from the TraPPE force field, while UFF Lennard-Jones parameters were used for the framework atoms. The framework atoms were assigned charges based on the EQeq[65] (extended charge equilibration) method. Although the framework flexibility may play an important role in some adsorption cases,[71–74] in this study the atomic positions were kept frozen during the simulations due to the unavailability of generic flexible force fields. The Lennard-Jones interactions were truncated at 12 Å without analytical tail correction, as is common in simulations for MOFs.[75,76] (Larger truncation distances do not lead to any significant change in selectivity, as shown in the Supporting Information.) The Ewald summation technique[77] was used with a relative precision of 10^{-6} for electrostatic interaction calculations. The GCMC simulations involved 50,000 cycles in total with equal equilibration and production cycles, where the allowed GCMC moves were translation, rotation, reinsertion,[78] molecular identity change, and random insertion/deletion with equal probability. Here, a Monte Carlo cycle is defined as max(20,N) Monte Carlo steps, in which N denotes the total number of O_2 and N_2 guest molecules in the simulation box. The gas loadings were computed in 5 blocks (i.e, for 1-10000, 10001-20000, …, 40001-50000 cycles). The ratios of gas uptake in the first and last simulation block over the average gas loading are plotted in Figure S8, which shows the insignificant deviations along the simulation. As a supplement, the average and variance of these ratios are presented in Table S11 where it can be seen that the averages over all materials are very similar in the first and last simulation blocks for both O_2 and N_2 and the spread of these ratios is narrow, which implies that 50,000 cycles were sufficient to get converged GCMC results.

Generation of Metalated Catecholate Functionalized Structures

Metalated MOF structures were created from the prescreened pristine MOFs (EDUVOO [IRMOF-14], RUBTAK02 [UiO-66(Zr)], SAHYIK [MOF-5], and Ce-UiO-66) by inserting only one metal-catecholate moiety in each potential metalation site (defined above under “Structural Analysis”). Ce-UiO-66 is not included in the CoRE MOF database, however, it has been added to our list of materials to study the effect of metal type in MOF nodes on binding energies, which was previously shown to be large for the binding energy of H_2O.[79] In this work, we report both the

refcode (i.e., a 6-character alphanumeric reference code) and common name for a MOF structure. Note that there might be multiple refcodes for a specific MOF depending on experimental conditions such as temperature, the presence of solvent molecules, etc. The geometry of the added metal-catecholate moiety was obtained from the DFT optimized geometry of N_2 bound to Zn-catecholate as published in previous work.[54] The MOF structures with metalated catecholates were checked for steric hindrances and symmetrical redundancy using an in-house code developed in Python, the procedure of which is detailed further below.

In the environmental analysis implemented in the code, a unit cell was expanded to a supercell with consideration of an environment checking radius of 15 Å for periodic boundary conditions. Next, within the checking radius centered on the added metal atom, up to 50 nearest framework atoms or more when distances of the atoms are too close (<0.05 Å) were selected to produce environment information for the specific metalation site. Four different characteristics were calculated as the environment information: atom type, distance between the added metal atom and the framework atom (r_{ij}), angle between the vector from the center of a ring to the added metal atom and the vector from the added metal atom to the framework atom (θ_1), and angle between the vector from one oxygen atom to the other oxygen atom in the catecholate ligand and the vector from the added metal atom to the framework atom (θ_2). Finally, based on the environment information, duplicate metalation sites were excluded (Figure 3). In addition, sterically unphysical metalation sites, which were too close to other framework atoms (<2.5 Å), were also filtered out.

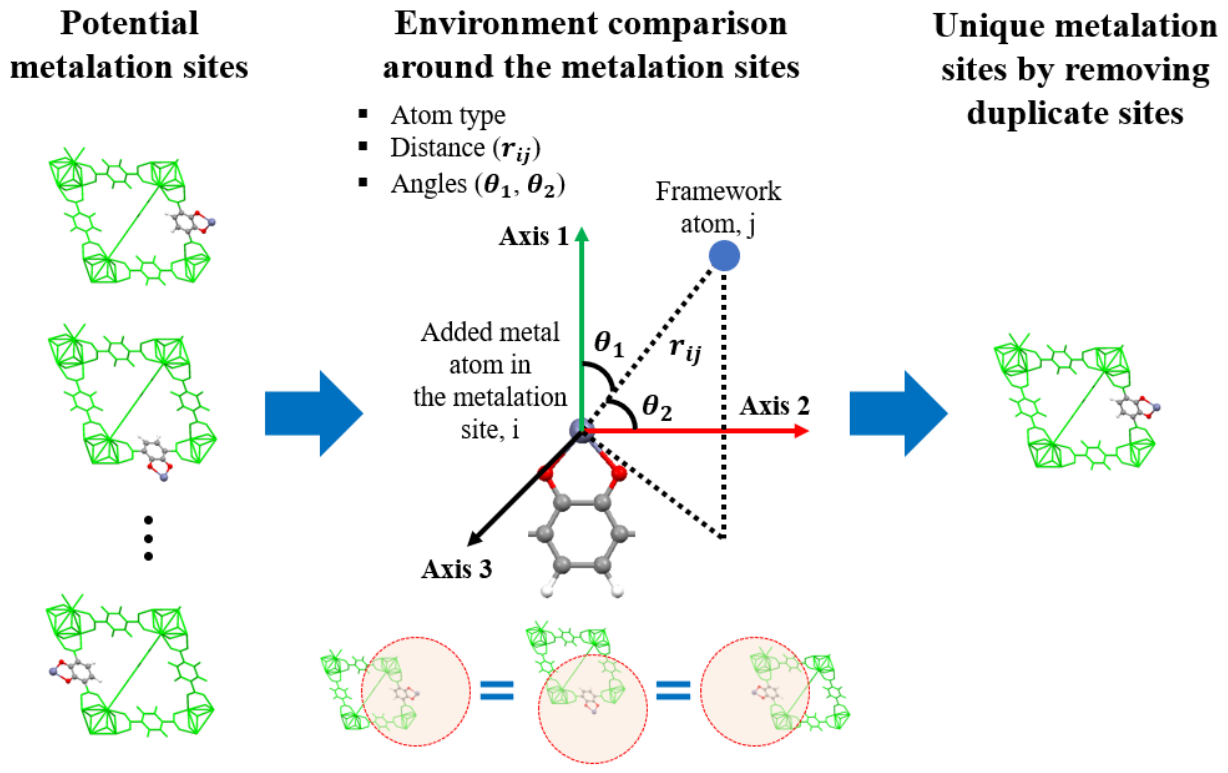

Figure 3. Environment comparison for identifying unique metalation sites among potential metalation sites.

Cluster DFT

Many different metals could be considered for the metal-catecholates, and treating each of them in each shortlisted MOF structure with periodic DFT would have required more calculations than could readily be performed. Instead, we chose a selected list of specific metals based on cluster calculations in previous work[54] and additional cluster DFT calculations using PBE-D3(BJ),[80–82] which allowed for direct comparison to periodic DFT results. In keeping with previous work,[54] the binding energies of guests (O_2 and N_2) to a given metal-catecholate were calculated as the energies of the isolated guest and the isolated metal-catecholate (Figure 4) subtracted from the energy of the catecholate-metal-guest supersystem (Equation 2).

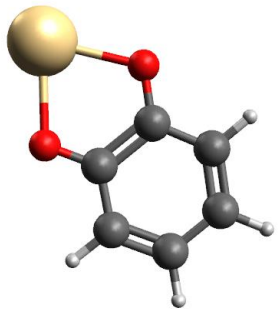

Figure 4. Cluster model of metal-catecholate system.

$$E_{bind} = E_{complex} - E_{metal-catecholate} - E_{adsorbate} \quad (2)$$

All new cluster DFT calculations were performed with Amsterdam Density Functional (ADF) 2017[83–85] using the all-electron TZ2P basis set[86] and the zeroth-order regular approximation (ZORA) for scalar relativity corrections.[87–89] All spin states were considered. The calculated Gibbs free energies are based on a standard state of ideal gas at 1 atm. For the sake of simplicity in the periodic DFT calculations, only 2+ oxidation states were considered for the data presented here. Metals were selected based on estimated availability of precursors and the likelihood of obtaining a 2+ oxidation state, specifically Be^{2+}, Mg^{2+}, Ca^{2+}, Cr^{2+}, Mn^{2+}, Fe^{2+}, Co^{2+}, Ni^{2+}, Zn^{2+}, Sr^{2+}, Pd^{2+}, Cd^{2+}, Ba^{2+}, Pt^{2+}, and Pb^{2+}.

Periodic DFT

The periodic spin-polarized DFT binding energies of O_2 and N_2 were calculated using the Vienna Ab Initio Simulation Package (VASP)[90,91] with PBE-D3(BJ).[80–82] In these calculations, both the MOF unit cell information and the MOF atomic coordinates were used as reported in the CoRE MOF database. A metal catecholate was incorporated into the viable MOFs (see Results and Discussion for details) and then the adsorbate molecules were initially placed near the metal catecholate in three orthogonal configurations and were then fully optimized. For Co and Ni in the metal-catecholates, high spin states were assumed for the metals with ferromagnetically coupled

O_2 in the framework. All periodic DFT calculations were performed using Γ-point sampling and a 500 eV kinetic energy cutoff. The energy and force convergence criteria were 10^{-5} eV and 0.01 eV/Å, respectively. Missing hydrogens in the RUBTAK02 structure were added as in Yang et al.[92] in order to have a neutral structure. The proton topology assigned for UiO-66(Zr) follows that of the most stable configuration of NU-1000 as demonstrated by Planas et al.[93] For periodic DFT calculations, the electronic binding energy is defined as:

$$E_{bind} = E_{complex} - E_{framework} - E_{adsorbate} \quad (3)$$

Results and Discussion

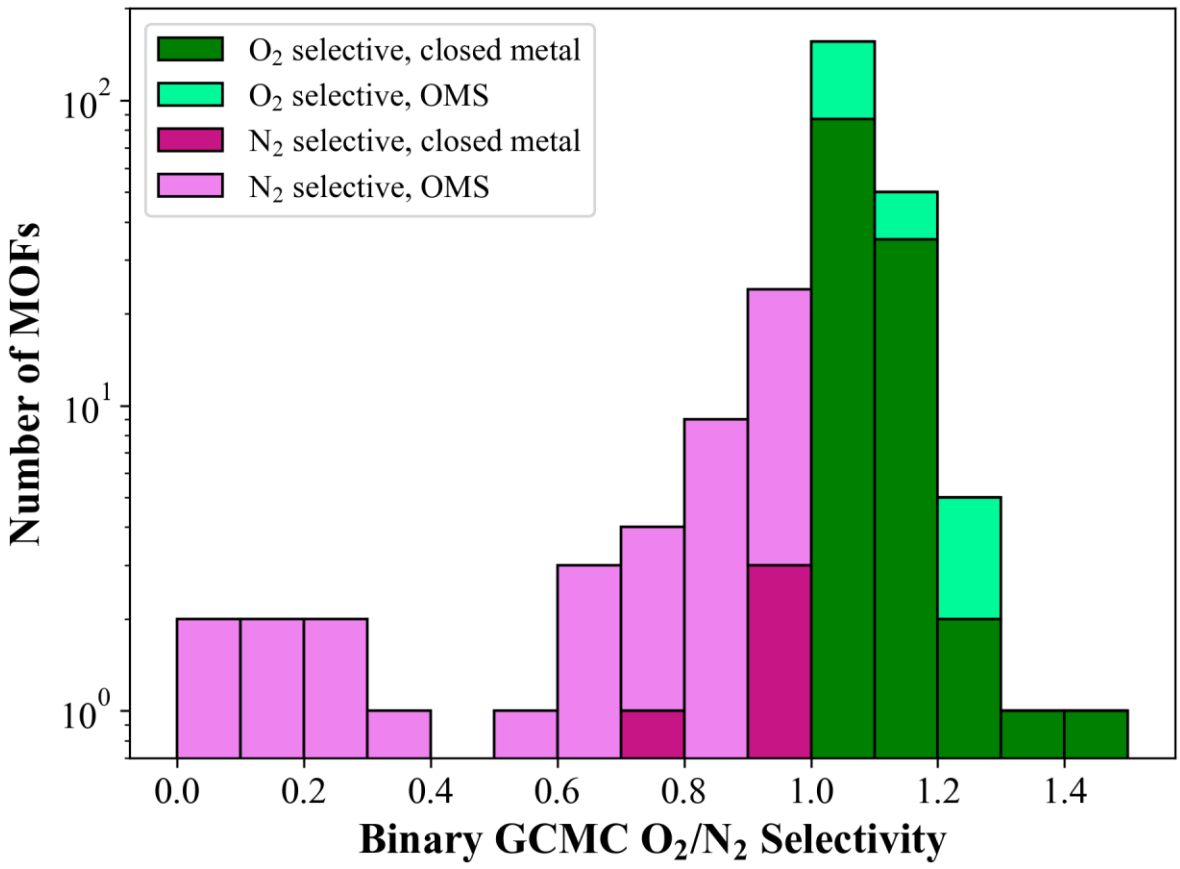

Figure 5. Binary GCMC O_2/N_2 (20%/80%) selectivity for 261 pristine MOFs obtained at 1 bar, 298 K.

In Figure 5, a histogram of the O_2/N_2 selectivities obtained from the binary GCMC simulations is shown for the 261 pristine MOFs. The selectivity varies between 0 and ~1.5, but most materials perform near a selectivity of 1. Unexpectedly, there are seven MOFs that show highly N_2 selective behavior ($0 < S_{O_2/N_2} < 0.4$), but all of these contain open metal sites. A more detailed analysis for NEXXEV, the most N_2 selective material, indicates that (after removal of solvent molecules) the structure contains rows of free (essentially uncoordinated) Li cations that cause erroneous partial charge assignments with the EQeq method and lead to unreasonably strong interactions with N_2 molecules (see Supporting Information). Detailed GCMC results can also be found in the Supporting Information.

Our screening analysis focuses on the materials that are O_2 selective ($S_{O_2/N_2} > 1$) based on the GCMC results. These materials have structural properties that allow preferential adsorption of O_2 over N_2, taking into account dispersion and electrostatic interactions only. However, it should be noted that the generic force fields (i.e. UFF) may fail to accurately account for the interactions between the sorbates and the adsorbent[32] for structures both with open metal sites (e.g., CO_2 adsorption in Mg-MOF-74[40]) and without open metal sites (e.g., Ar adsorption in ZIF-8[39]). Thus, in reality, these O_2 selective materials could exhibit higher selectivity than predicted by GCMC simulations. For example, the experimental O_2/N_2 selectivity is calculated as ~1.7, and ~1.7-1.8 for UMCM-1, and MOF-177, respectively, by taking the ratio of pure O_2 and N_2 adsorption loadings at 298 K, 1 bar.[52] To test the proximity of UFF predictions with respect to experiments, we performed pure O_2 and N_2 GCMC simulations and the O_2/N_2 selectivity is predicted to be 1.05 and 1.02 for UMCM-1 and MOF-177, respectively. Our conclusions match those of Zeitler et al.,[36] who found that UFF failed to account for O_2-metal interactions in a study comparing the experimental O_2/N_2 selectivities of several MOFs to those obtained by GCMC simulations . Thus, the calculated GCMC O_2/N_2 selectivities in this work likely underpredict O_2/N_2 selectivity that would be obtained in experimental conditions. Accordingly, it should not be assumed that the GCMC step of the screening identifies that the best candidates without further screening being necessary. On the contrary, the GCMC step only eliminates the cases that would be N_2-selective, which would be counterproductive for O_2-selective modifications.

To obtain a more accurate description of O_2 and N_2 adsorption, periodic DFT calculations were performed on the metal-catecholated versions of a subset of these materials. Considering only cases for which $S_{O_2/N_2} > 1$ left 210 surviving MOF structures out of the original 5,109 for possible metalation. From these 210 structures, a total of 4,977 potential metalated structures can be generated by assuming every two adjacent H atoms in the rings can be transformed to a metal-catecholate complex, and by including only one metalation site per metalated structure. However, to perform DFT calculations for all the generated potential metalated structures would be a daunting task, especially as there would need to be at least 7 calculations per metalated structure: with and without two different gas molecules, N_2 and O_2, and with 3 different initial configurations for each (see Figure 6).

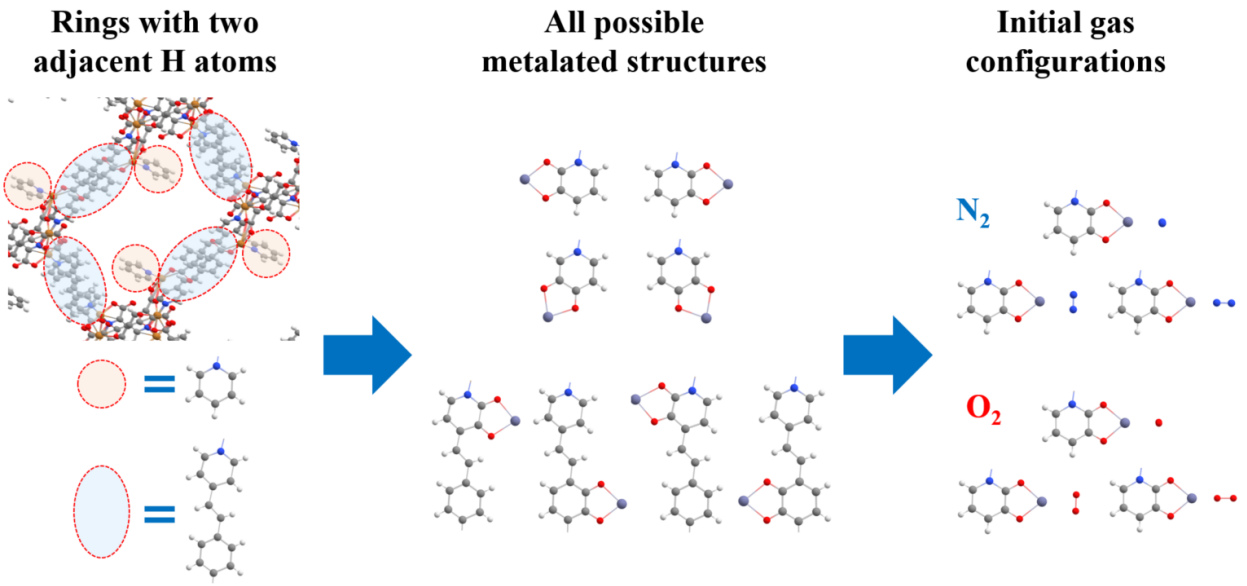

Figure 6. Generation of metalated structures for the periodic DFT calculations. Color code: oxygen atoms, red; carbon, gray; hydrogen, white; nitrogen, blue; metal, blue-gray.

To narrow down the number of potential metalated structures for further DFT calculations, metalated structures with duplicate or sterically unrealistic metalation sites were excluded via environment comparisons (Figure 3) using in-house developed code. Unrealistic metalation sites could be created when the added metalation site is in a small pore, or the direction of the metal-catecholate complex (i.e., direction from the center of a ring to the added metal atom) faces toward the pore wall (see Supporting Information for details). Note that this set of exclusions is therefore physically motivated, not merely a concession to computational limits.

Following the environment comparisons, 564 unique metalated structures from 168 parent MOF structures were obtained. To simplify the analysis, MOF structures that possess more than one unique metalation site are ruled out. MOFs with multiple unique metalation sites would likely have an unpredictable mixture of metalated sites in experiment, making it more difficult to make comparisons between experiment and theory. While it is possible that some of the excluded structures could yield even better air separation capabilities than those we consider for the remainder of this study, our focus on this work is identifying several promising candidates in such a way that the computational results can be experimentally tested.

Of the 564 possible metalated structures, only 55 have only one unique metalation site. In these structures, the structure nodes feature different metals: Cd (1), Cu (8), Mn (2), Sc (1), Zn (41), and Zr (2), where the number in the parentheses is the number of structures. 55 structures would still have led to an overabundance of calculations, so we attempted to select a diverse sample by considering at least one MOF with each metal in the node for DFT optimization after the metal catecholate incorporation. However, we observe that for many structures incorporation of the metal catecholate led to large structural changes during the optimization (e.g., for UKIQIP-Zn-cat the Zn of the catecholate unit is found to approach closely the C atoms of the nearest benzene

ring), and we surmise that these structures would not be stable in their metal catecholate form. In general, we have observed that converging to a physically reliable structure (i.e. no undesired bond breakage/formation) becomes harder as the metalated linker points more towards the MOF scaffold rather than the open porous space. In those cases, the strong confinement effect around the metalated linkers may be responsible for the significant distortion of the structure. We have not investigated the effect of the orientation of the metalated linker on the optimization of the structures, however, as it is beyond the scope of our screening study. For simplicity, our metalated structure optimizations are initialized with the same orientation of the linkers as in the pristine MOFs. Only SAHYIK (Zn)-M-cat, EDUVOO (Zn)-M-cat, and RUBTAK02 (Zr)-M-cat resulted in functional structures after optimization (SAHYIK: $Zn_4O(BDC)_3$, where BDC = 1,4-benzene-dicarboxylate, EDUVOO: $Zn_4O(PDC)_3$ where PDC = pyrene-2,7-dicarboxylate, RUBTAK02 (H atoms added): $Zr_6O_4(OH)_4(BDC)_6$) where the interatomic distances are reliable with no undesired bond formation/breakage. The vibrational frequency calculations of the optimized structures are not performed due to the high computational cost. It is notable that these MOFs have large pores where the metalated linkers are oriented towards the pore space. The structures identified using the screening methodology are listed with their structural information in Table 1 for parent and metal-catecholated MOFs with 5 different metals in catecholates that will be discussed in the next paragraph. Note that UiO-66(Zr) (here as RUBTAK02) has been successfully used before as a support for metalated catecholates.[58,59] As expected, with the addition of metal catecholates, there are slight decreases in void fractions. However, in terms of pore sizes, the incorporation of metal catecholate can cause an increase or decrease depending on the rotation of the linker in the optimized structures.

Table 1. Final MOF candidates studied for O_2/N_2 separation.

MOF	Metal node	Metal-catecholate	PLD (Å)	LCD (Å)	Void fraction
SAHYIK (MOF-5)	Zn	-	7.8	14.9	0.77
		Cd	8.0	15.1	0.76
		Co	8.0	15.2	0.76
		Mg	8.0	15.1	0.76
		Ni	8.0	15.2	0.76
		Zn	8.0	15.2	0.76
EDUVOO (IRMOF-14)	Zn	-	10.6	20.9	0.84
		Cd	10.4	21.0	0.83
		Co	10.4	21.0	0.83
		Mg	10.4	21.0	0.83
		Ni	10.5	21.0	0.83
		Zn	10.4	21.0	0.83
RUBTAK02 (UiO-66)	Zr	-	3.9	8.5	0.47
		Cd	4.2	7.7	0.44
		Co	4.2	7.7	0.43
		Mg	4.2	7.7	0.44
		Ni	4.2	7.7	0.45

		Zn	4.2	7.7	0.45
UiO-66	Ce	-	4.4	9.1	0.50
		Cd	4.5	8.1	0.48
		Co	4.5	8.1	0.47
		Mg	4.5	8.1	0.48
		Ni	4.5	8.1	0.48
		Zn	4.5	8.1	0.49

In selecting the candidate metals for the metal-catecholates, it is important to strike a balance between the absolute O_2 binding energy, which is important for reversibility, and the difference in O_2 and N_2 binding energies ($E_{sep} = E_{b, O2} - E_{b, N2}$), which speaks to potential for separation. In the previous cluster calculations[54] all metals other than Cu (i.e, Mg, Sc, Ti, V, Cr, Mn, Fe, Co, Ni, and Zn) were predicted to be O_2 selective and had high values for E_{sep}, but were also predicted to have extremely high absolute O_2 binding that would likely be irreversible. In order to see whether the magnitude of the O_2 binding might decrease at the periodic level, we selected the cases with the (relatively) weakest O_2 binding among the investigated metals above: Co, Mg, Ni, and Zn. However, when their periodic DFT binding energies were calculated in this work, they were found to be similar to the cluster DFT binding energies and therefore still have very strong absolute O_2 binding energies (in the Supporting Information, Table S3). Therefore, for this study we performed new cluster calculations on a larger set of metals in order to identify more favorable metal candidates. As explained in the Computational Methods section, these metals were selected for their expected experimental feasibility based on the availability of synthetic precursors and accessibility of the 2+ oxidation state. The results of the new cluster calculations are presented in Figure 7, and as before, most metals studied are predicted to have overly strong binding for O_2. There is not necessarily a known specific value for the electronic binding energy below which O_2 binding will be reversible, in part because it would depend on the thermal stability of the specific MOF support. However, we expect that ideally the absolute O_2 binding energies would need to be within ~20-40 kJ/mol, and therefore in order to obtain good O_2/N_2 separation the absolute N_2 binding energies would ideally be near 0 kJ/mol so as to maintain a maximum differential. Of the metals studied, only Cd and Pb offer sufficiently low absolute N_2 binding energies. In Cd-catecholate, the difference between O_2 and N_2 binding energy is substantial, which suggests N_2 may not compete with O_2. This competitive advantage is not expected to hold for Pb-catecholate due to the smaller difference between O_2 and N_2 binding energies. In light of these factors, Pb catecholates are not considered further, and the final list of metals for the metal-catecholates is Cd, Co, Mg, Ni, and Zn. We acknowledge that all of these metals feature absolute O_2 binding energies larger than 40 kJ/mol, but as we discuss further down we believe there are mitigating factors that keep Cd within the realm of practical possibilities. While Co, Mg, Ni, and Zn all have much larger absolute O_2 binding energies and are not expected to allow for reversible binding, we include their periodic DFT results for the sake of analyzing whether binding trends are exclusively due to the metals in the metal-catecholates or whether the support structures also play a role.

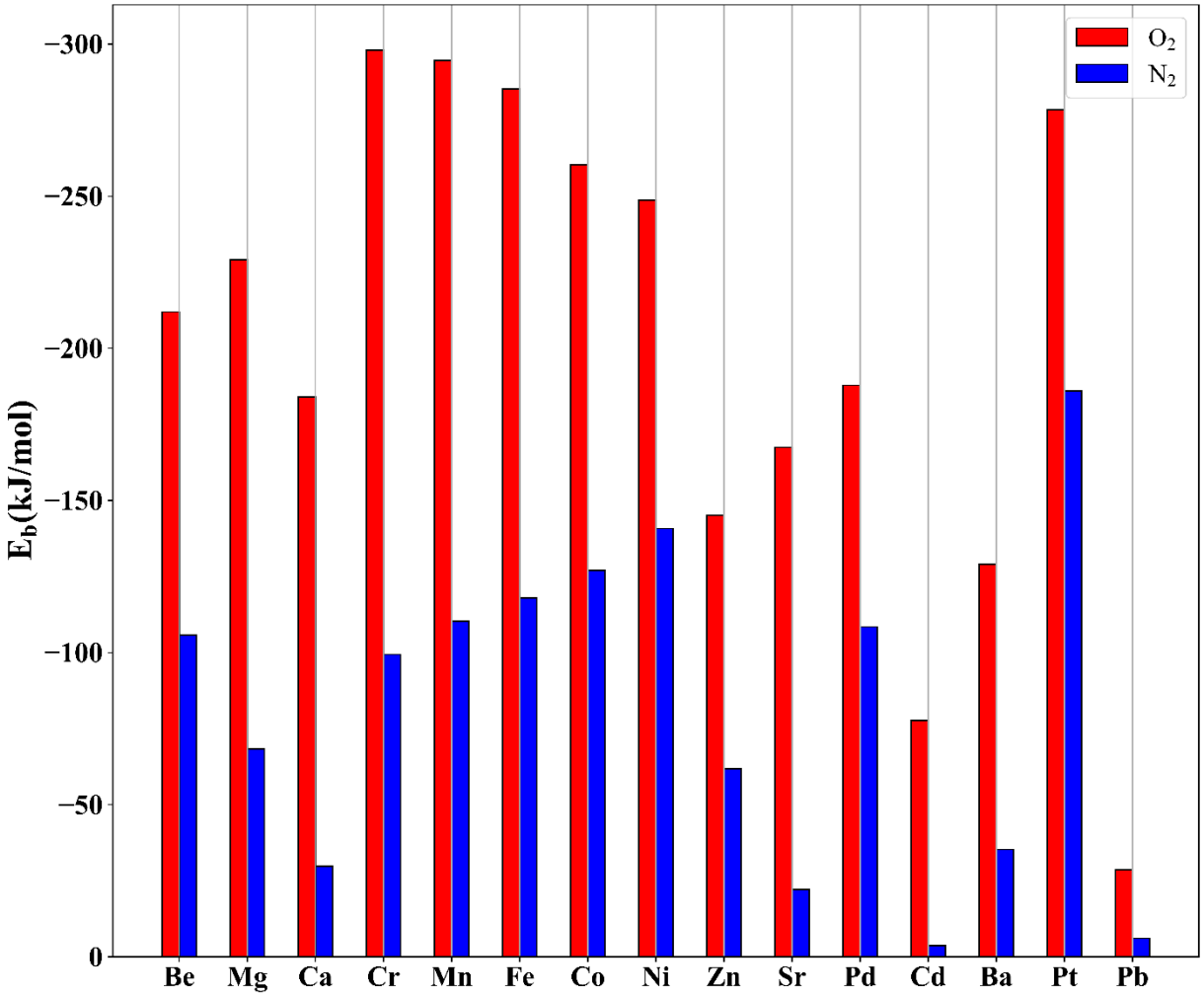

Figure 7. PBE-D3(BJ) binding energies (E_b) of O_2 and N_2 in cluster models. Results presented here use the lowest energy spin state for each system.

The selected metal-catecholates are included in four MOFs to obtain the binding energies using periodic DFT. Those binding energies are then compared with those from cluster models. Figure 8 presents O_2 and N_2 binding energies for each material, where the type of metal-catecholate is denoted with a suffix after the MOF name (i.e. MOF Name-Zn-cat). The binding energies shown in Figure 8 are calculated with the lowest energy configurations optimized from the three orthogonal initial positions. Note that the MOF structure (i.e. the environment of the metal catecholate) has limited effect on the strength of O_2 and N_2 adsorption, as can be seen when comparing data with the same metal-catecholates in different MOFs. However, it should be indicated that a different observation is possible for other MOFs, especially MOFs having smaller pores that create larger confinement effects around the adsorbate. Such an effect does not exist in the studied structures due to the distance of the atoms (except the metal catecholate) around the adsorbates. Besides the full framework effect, it should also be noted that the binding energies of

O_2 and N_2 change very little when comparing between UiO-66(Zr) and its Ce analogue, implying that the effect of the metal in the node is minimal when the binding is taking place at a metal-catecholate inserted into a linker. The nature of the support structure, however, may remain relevant in that some degree of thermal stability will be required in order to maintain structural integrity during the adsorption and release of O_2. The strength of O_2 adsorption follows the order of Mg-cat > Co-cat > Ni-cat ≈ Zn-cat > Cd-cat while N_2 adsorption strength is in the order of Ni-cat ≈ Co-cat > Mg-cat ≈ Zn-cat > Cd-cat. To estimate the O_2/N_2 selectivity in periodic systems, the following relation is used:

$$S_{O2/N2,DFT} = e^{-(\Delta G_{O_2} - \Delta G_{N_2})/RT} \quad (4)$$

Here, $\Delta G = \Delta E + \Delta G_{corr}$ where ΔE is the electronic binding energy obtained in the periodic model and ΔG_{corr} is the difference between ΔG and ΔE obtained from the cluster calculations. As can be seen in Table S10, $S_{O2/N2,DFT}$ follows the order: Mg-cat > Zn-cat > Cd-cat > Co-cat > Ni-cat for all MOF types. It should be noted that $S_{O2/N2,DFT}$ is only a qualitative value that is used to give an idea about the selectivity trends at low pressure. It should not be considered a quantitative value for selectivity (i.e. $S_{O2/N2,DFT}$ value of 0.3 for SAHYIK-Ni-cat does not imply that structure is N_2 selective, it rather demonstrates that, among SAHYIK materials, SAHYIK-Ni-cat is predicted to be the least selective since others possess higher selectivity estimates.)

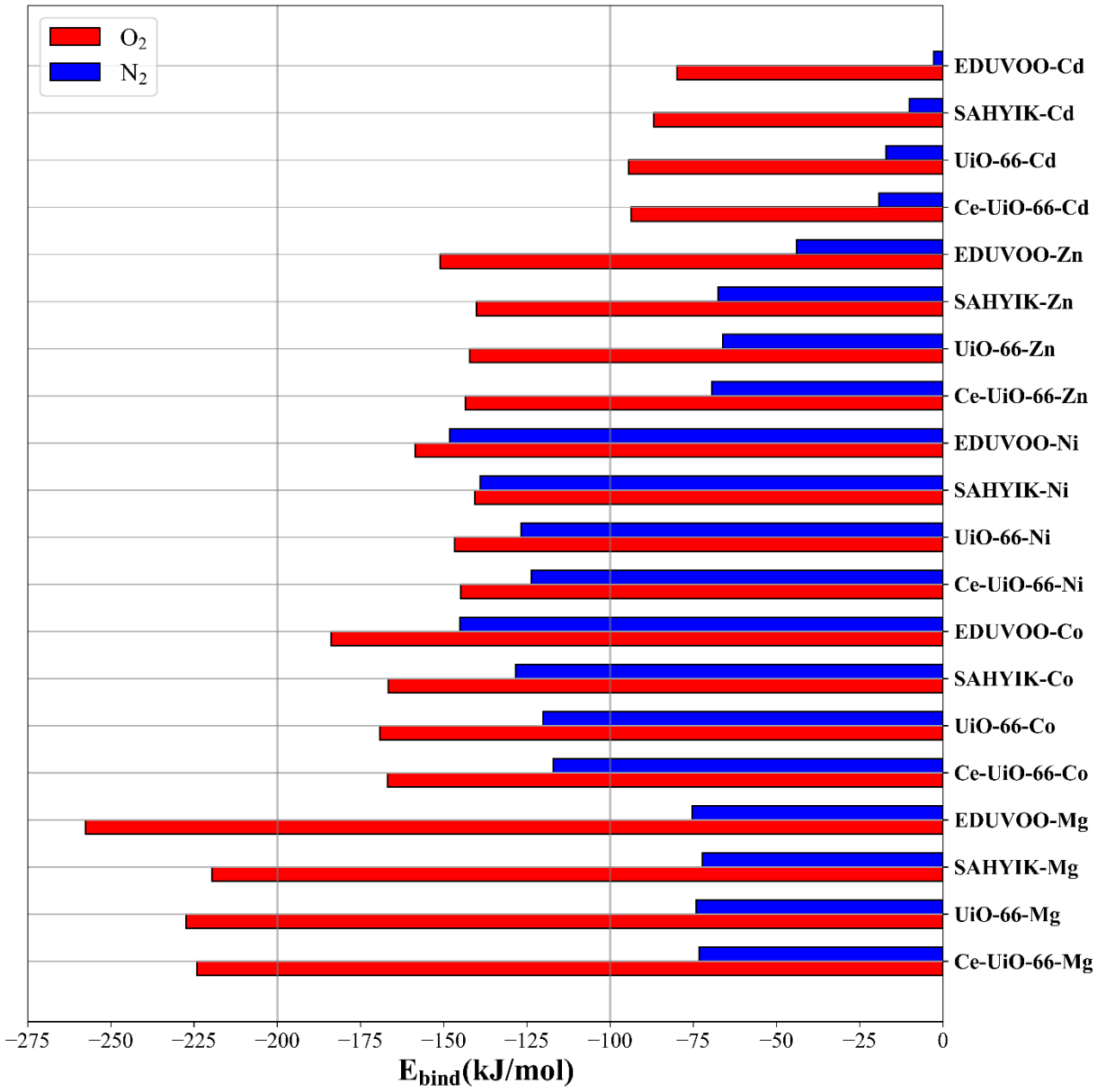

Figure 8. PBE-D3(BJ) binding energies (E_b) of O_2 and N_2 in RUBTAK02 (UiO-66), Ce-UiO-66, SAHYIK (MOF-5), and EDUVOO (IRMOF-14) incorporated with metal-catecholates (Mg, Co, Ni, Zn, and Cd).

In order to rationalize the binding energy trends, we further analyzed our periodic results for EDUVOO MOF and calculated Quantum Theory of Atoms in Molecules (QTAIM) charges using the Bader charge analysis code developed by the Henkelman Group at the University of Texas – Austin[94–98] on the catecholate metal center and on the bonded O_2/N_2 molecules. We do not see a significant difference in the QTAIM charges of metal centers when comparing between the three different guest conformations, so the QTAIM charges of the metal centers are reported for the most

stable conformations only (in the Supporting Information, Table S9). We note that while charge is an important electrostatic descriptor, there is another key difference between these metals, namely that the Co and Ni metals have partially filled *d* orbital shells while Mg, Zn, and Cd are characterized by all shells of a given angular momentum being fully filled. We found that for Mg, Zn, and Cd, the QTAIM charge on the metal center follows the same order as that of the binding energy (i.e. Mg > Zn > Cd). For Co and Ni, we observed that for Co-catechol the QTAIM charge on the Co center is slightly higher than that of the Ni in the O_2-bound catechol, suggesting that O_2 binds slightly stronger to the Co-catechol compared to the Ni-catechol because it oxidizes the metal to a greater extent. The charges on the Co and Ni centers are very similar in the N_2 bounded structures and thus their N_2 binding energies are very similar as well.

The periodic results mirror those reported for cluster calculations in previous work[54] because the large pores result in there not being a significant adsorption site near the adsorbate other than the metal catecholate. Zn-cat had lower absolute O_2 and N_2 binding energies than most of the other metals studied due to a full 3*d* subshell that minimizes covalency in O_2 or N_2 binding. In our current work, we see that Cd has even lower absolute O_2 and N_2 binding energies than Zn; this is consistent with the more diffuse character of the Cd 5*s* orbital compared to the 4*s* for Zn, which leads to the guests binding at greater distances and with reduced electrostatic interactions as well as reduced overlap for any covalent contributions to binding.

While a significant difference between O_2 and N_2 binding energies in favor of O_2 adsorption would be beneficial for efficient O_2/N_2 separation, absolute O_2 binding energies cannot be too large without causing a high energy requirement for regeneration. O_2 and N_2 binding energies in MOFs with Mg-catecholate suggest that, in spite of the large E_{sep}, they are not the ideal materials due to having overly high absolute O_2 binding energies (over 220 kJ/mol). MOFs with other metal-catecholates also exhibit high absolute O_2 adsorption energies (~80-180 kJ/mol) despite being lower than those in MOFs with Mg-catecholates. Within the five metal catecholates studied with periodic DFT, Cd-catecholates lead to the lowest absolute O_2 adsorption energies in MOFs (~80-95 kJ/mol) together with low absolute N_2 adsorption energies (~3-20 kJ/mol). Even at 80 kJ/mol, however, it would likely be difficult to evacuate O_2 from the material at low pressures, which would lead to a high regeneration cost when using these MOFs to separate an O_2/N_2 mixture. That being said, there are several possible solutions. In this work, the adsorption energies of only the first molecules adsorbed are investigated in detail. However, it is likely that many of the subsequent molecules would adsorb with less energy, which can render a material partially regenerable. This hypothesis is best tested using MOFs with Cd-catecholates, as their O_2 adsorption is expected to be weaker than the other materials. To illustrate this idea, DFT calculations employing two O_2 molecules near the Cd-catecholate of EDUVOO have been performed with different initial positions selected for O_2 molecules. The lowest energy configuration shows a combined binding energy for two O_2 molecules to be -110.4 kJ/mol, or an average of -65.2 kJ/mol. As the lowest binding energy for the first O_2 molecule in EDUVOO-Cd-Cat is -79.9 kJ/mol, this implies that a second O_2 molecule will have weaker binding than the first one. Furthermore, it may be possible to weaken the intensity of the O_2 binding by further functionalization of the catecholate carbon ring. Zhang et al. have found that the redox capabilities of a metal-catecholate can be tuned by adding functional groups to the opposite side of the 6-membered ring.[61] While their study was for catalysis, it is possible that a similar strategy could be used for gas separation. Because tuning the redox activity would likely proceed by adding

functional groups to the 6-membered ring according to established principles of organic chemistry, our current work should serve as a useful starting point for any such future studies.

Conclusions

Air separation has long been an active research topic because oxygen and nitrogen are highly desired gases for many industries and applications. In contrast to earlier N_2-selective zeolite studies, this work focuses on the potentially O_2-selective MOFs. O_2-selective materials are more economically desirable for high-purity and high-volume oxygen due to requiring lower volumes of processed gas in a real application. The MOFs that are investigated in this work (RUBTAK02 (UiO-66(Zr)), SAHYIK (MOF-5), and EDUVOO (IRMOF-14)) are shortlisted from the CoRE MOF database using structural criteria and binary GCMC O_2/N_2 selectivity data. Ce-UiO-66 is also added to this list despite not being a constituent of the CoRE MOF database in order to study the effect of metals in UiO-66 nodes on adsorption energies. These MOFs are modified with metal catecholates (Mg, Co, Ni, Zn, and Cd) to investigate O_2 and N_2 binding affinity using DFT. In general, the change in O_2 and N_2 binding energies across different MOFs is small, implying the dominant factor to be the metal type in the metal catecholate and that the MOF structure has only a secondary effect on the binding energies. This suggests that, in most of the cases, the interaction of sorbates near metal catecholates is dominant over other moieties in the structure. Since overly strong adsorption is not favored for regenerability, materials that have relatively low absolute O_2 binding energies are sought, along with low absolute N_2 binding energies for high O_2/N_2 selectivity. Out of five metal catecholates, Cd-catecholates show the least intense O_2 adsorption (~80-95 kJ/mol), and with much less favorable N_2 adsorption (~3-20 kJ/mol). The big difference between O_2 and N_2 binding energies could enable high O_2/N_2 selectivity, however, due to the relatively high O_2 binding energies, MOFs with Cd-catecholates likely would experience regenerability problems. It is possible, however, that in practice O_2 binding would be weaker than predicted due to anions or solvents such as water binding to the metal, increasing the coordination number. It also may be possible to tune the binding energies by modifying the catecholate carbon ring. Although it is not studied in this work, another approach could be using these MOFs for catalysis, where these materials might provide a suitable medium for oxidation of molecules such as methane or ethane.

Acknowledgments

This research is supported by the U.S. Department of Energy, Office of Basic Energy Sciences, Division of Chemical Sciences, Geosciences and Biosciences under Award DEFG02–17ER16362. Computer resources were provided by the Minnesota Supercomputing Institute at the University of Minnesota.

Supporting Information

Breakdown of numbers of atoms in size-eliminated MOFs; detailed GCMC simulation results; neutrality check for MOFs; metalation code details; DFT binding energies and associated absolute

energies in cluster and periodic models; analysis of the most N_2 selective MOF; analysis of the sensitivity of GCMC O_2/N_2 selectivities to Lennard-Jones cutoff distances; periodic DFT on two O_2 molecules in EDUVOO-Cat-Cd; gas loadings across the GCMC simulation blocks.

References

(1) Bloch, E. D.; Murray, L. J.; Queen, W. L.; Chavan, S.; Maximoff, S. N.; Bigi, J. P.; Krishna, R.; Peterson, V. K.; Grandjean, F.; Long, G. J.; et al. Selective Binding of O2 over N2 in a Redox–Active Metal–Organic Framework with Open Iron(II) Coordination Sites. *J. Am. Chem. Soc.* **2011**, *133*, 14814–14822.

(2) Fernández-Barquín, A.; Casado-Coterillo, C.; Valencia, S.; Irabien, A. Mixed Matrix Membranes for O2/N2 Separation: The Influence of Temperature. *Membranes (Basel, Switz.).* **2016**, *6*, 28.

(3) Santos, J. C.; Cruz, P.; Regala, T.; Magalhães, F. D.; Mendes, A. High-Purity Oxygen Production by Pressure Swing Adsorption. *Ind. Eng. Chem. Res.* **2007**, *46*, 591–599.

(4) Ferreira, D.; Boaventura, M.; Bárcia, P.; Whitley, R. D.; Mendes, A. Two-Stage Vacuum Pressure Swing Adsorption Using AgLiLSX Zeolite for Producing 99.5+% Oxygen from Air. *Ind. Eng. Chem. Res.* **2016**, *55*, 722–736.

(5) Kim, M.-B.; Jee, J.-G.; Bae, Y.-S.; Lee, C.-H. Parametric Study of Pressure Swing Adsorption Process To Purify Oxygen Using Carbon Molecular Sieve. *Ind. Eng. Chem. Res.* **2005**, *44*, 7208–7217.

(6) Jeong-Geun, J.; Sang-Jin, L.; Min-Bae, K.; Chang-Ha, L. Three-bed PVSA Process for High-purity O2 Generation from Ambient Air. *AIChE J.* **2005**, *51*, 2988–2999.

(7) Kather, A.; Scheffknecht, G. The Oxycoal Process with Cryogenic Oxygen Supply. *Naturwissenschaften* **2009**, *96*, 993–1010.

(8) Adil, K.; Belmabkhout, Y.; Pillai, R. S.; Cadiau, A.; Bhatt, P. M.; Assen, A. H.; Maurin, G.; Eddaoudi, M. Gas/Vapour Separation Using Ultra-Microporous Metal-Organic Frameworks: Insights into the Structure/Separation Relationship. *Chem. Soc. Rev.* **2017**, *46*, 3402–3430.

(9) Rege, S. U.; Yang, R. T. Limits for Air Separation by Adsorption with LiX Zeolite. *Ind. Eng. Chem. Res.* **1997**, *36*, 5358–5365.

(10) Baksh, M. S. A.; Kikkinides, E. S.; Yang, R. T. Lithium Type X Zeolite as a Superior Sorbent for Air Separation. *Sep. Sci. Technol.* **1992**, *27*, 277–294.

(11) Zanota, M.-L.; Heymans, N.; Gilles, F.; Su, B.-L.; De Weireld, G. Thermodynamic Study of LiNaKLSX Zeolites with Different Li Exchange Rate for N2/O2 Separation Process. *Microporous Mesoporous Mater.* **2011**, *143*, 302–310.

(12) Jayaraman, A.; Yang, R. T. Stable Oxygen-Selective Sorbents for Air Separation. *Chem. Eng. Sci.* **2005**, *60*, 625–634.

(13) Lee, S.-J.; Jung, J.-H.; Moon, J.-H.; Jee, J.-G.; Lee, C.-H. Parametric Study of the Three-Bed Pressure−Vacuum Swing Adsorption Process for High Purity O2 Generation from

Ambient Air. *Ind. Eng. Chem. Res.* **2007**, *46*, 3720–3728.

(14) Nolan, J. T.; McKeehan, T. W.; Danner, R. P. Equilibrium Adsorption of Oxygen, Nitrogen, Carbon Monoxide, and Their Binary Mixtures on Molecular Sieve Type 10X. *J. Chem. Eng. Data* **1981**, *26*, 112–115.

(15) Kim, Y. H.; Lee, D. G.; Moon, D. K.; Byeon, S.-H.; Ahn, H. W.; Lee, C. H. Effect of Bed Void Volume on Pressure Vacuum Swing Adsorption for Air Separation. *Korean J. Chem. Eng.* **2014**, *31*, 132–141.

(16) Potoff, J. J.; Siepmann, J. I. Vapor–Liquid Equilibria of Mixtures Containing Alkanes, Carbon Dioxide, and Nitrogen. *AIChE J.* **2001**, *47*, 1676–1682.

(17) Zhang, L.; Siepmann, J. I. Direct Calculation of Henry's Law Constants from Gibbs Ensemble Monte Carlo Simulations: Nitrogen, Oxygen, Carbon Dioxide and Methane in Ethanol. *Theor. Chem. Acc.* **2006**, *115*, 391–397.

(18) Richards, A. J.; Watanabe, K.; Austin, N.; Stapleton, M. R. Computer Simulation of the Gas Separation Properties of Zeolite Li-X. *J. Porous Mater.* **1995**, *2*, 43–49.

(19) Susumu, K.; Ryo, K.; Shin-ichiro, N. Functional Porous Coordination Polymers. *Angew. Chemie Int. Ed.* **2004**, *43*, 2334–2375.

(20) Yaghi, O. M.; O'Keeffe, M.; Ockwig, N. W.; Chae, H. K.; Eddaoudi, M.; Kim, J. Reticular Synthesis and the Design of New Materials. *Nature* **2003**, *423*, 705.

(21) Férey, G. Hybrid Porous Solids: Past, Present, Future. *Chem. Soc. Rev.* **2008**, *37*, 191–214.

(22) Furukawa, H.; Cordova, K. E.; O'Keeffe, M.; Yaghi, O. M. The Chemistry and Applications of Metal-Organic Frameworks. *Science.* **2013**, *341*, 974.

(23) Wilmer, C. E.; Leaf, M.; Lee, C. Y.; Farha, O. K.; Hauser, B. G.; Hupp, J. T.; Snurr, R. Q. Large-Scale Screening of Hypothetical Metal-Organic Frameworks. *Nat. Chem.* **2012**, *4*, 83–89.

(24) Groom, C. R.; Bruno, I. J.; Lightfoot, M. P.; Ward, S. C. The Cambridge Structural Database. *Acta Crystallogr. Sect. B* **2016**, *72*, 171–179.

(25) Chung, Y. G.; Camp, J.; Haranczyk, M.; Sikora, B. J.; Bury, W.; Krungleviciute, V.; Yildirim, T.; Farha, O. K.; Sholl, D. S.; Snurr, R. Q. Computation-Ready, Experimental Metal–Organic Frameworks: A Tool To Enable High-Throughput Screening of Nanoporous Crystals. *Chem. Mater.* **2014**, *26*, 6185–6192.

(26) Colón, Y. J.; Gómez-Gualdrón, D. A.; Snurr, R. Q. Topologically Guided, Automated Construction of Metal–Organic Frameworks and Their Evaluation for Energy-Related Applications. *Cryst. Growth Des.* **2017**, *17*, 5801–5810.

(27) Smit, B.; Maesen, T. L. M. Molecular Simulations of Zeolites: Adsorption, Diffusion, and Shape Selectivity. *Chem. Rev.* **2008**, *108*, 4125–4184.

(28) Watanabe, T.; Sholl, D. S. Accelerating Applications of Metal–Organic Frameworks for Gas Adsorption and Separation by Computational Screening of Materials. *Langmuir* **2012**,

28, 14114–14128.

(29) Patrick, R.; K., F. O.; J., B. L.; Q., S. R. Computational Screening of Metal-organic Frameworks for Xenon/Krypton Separation. *AIChE J.* **2010**, *57*, 1759–1766.

(30) Moghadam, P. Z.; Islamoglu, T.; Goswami, S.; Exley, J.; Fantham, M.; Kaminski, C. F.; Snurr, R. Q.; Farha, O. K.; Fairen-Jimenez, D. Computer-Aided Discovery of a Metal–Organic Framework with Superior Oxygen Uptake. *Nat. Commun.* **2018**, *9*, 1378.

(31) DeCoste, J. B.; Weston, M. H.; Fuller, P. E.; Tovar, T. M.; Peterson, G. W.; LeVan, M. D.; Farha, O. K. Metal-Organic Frameworks for Oxygen Storage. *Angew. Chemie - Int. Ed.* **2014**, *53*, 14092–14095.

(32) Fang, H.; Demir, H.; Kamakoti, P.; Sholl, D. S. Recent Developments in First-Principles Force Fields for Molecules in Nanoporous Materials. *J. Mater. Chem. A* **2014**, *2*, 274–291.

(33) Basdogan, Y.; Keskin, S. Simulation and Modelling of MOFs for Hydrogen Storage. *CrystEngComm* **2015**, *17*, 261–275.

(34) Assfour, B.; Seifert, G. Hydrogen Storage in 1D Nanotube-like Channels Metal–Organic Frameworks: Effects of Free Volume and Heat of Adsorption on Hydrogen Uptake. *Int. J. Hydrogen Energy* **2009**, *34*, 8135–8143.

(35) Lennox, M. J.; Bound, M.; Henley, A.; Besley, E. The Right Isotherms for the Right Reasons? Validation of Generic Force Fields for Prediction of Methane Adsorption in Metal-Organic Frameworks. *Mol. Simul.* **2017**, *43*, 828–837.

(36) Zeitler, T. R.; Van Heest, T.; Sholl, D. S.; Allendorf, M. D.; Greathouse, J. A. Predicting Low-Pressure O2 Adsorption in Nanoporous Framework Materials for Sensing Applications. *ChemPhysChem* **2013**, *14*, 3740–3750.

(37) Rappe, A. K.; Casewit, C. J.; Colwell, K. S.; Goddard, W. A.; Skiff, W. M. UFF, a Full Periodic Table Force Field for Molecular Mechanics and Molecular Dynamics Simulations. *J. Am. Chem. Soc.* **1992**, *114*, 10024–10035.

(38) Mercado, R.; Vlaisavljevich, B.; Lin, L.-C.; Lee, K.; Lee, Y.; Mason, J. A.; Xiao, D. J.; Gonzalez, M. I.; Kapelewski, M. T.; Neaton, J. B.; et al. Force Field Development from Periodic Density Functional Theory Calculations for Gas Separation Applications Using Metal–Organic Frameworks. *J. Phys. Chem. C* **2016**, *120*, 12590–12604.

(39) Demir, H.; Greathouse, J. A.; Staiger, C. L.; Perry IV, J. J.; Allendorf, M. D.; Sholl, D. S. DFT-Based Force Field Development for Noble Gas Adsorption in Metal Organic Frameworks. *J. Mater. Chem. A* **2015**, *3*, 23539–23548.

(40) Dzubak, A. L.; Lin, L.-C.; Kim, J.; Swisher, J. A.; Poloni, R.; Maximoff, S. N.; Smit, B.; Gagliardi, L. Ab Initio Carbon Capture in Open-Site Metal–Organic Frameworks. *Nat Chem* **2012**, *4*, 810–816.

(41) Coudert, F.-X.; Fuchs, A. H. Computational Characterization and Prediction of Metal–Organic Framework Properties. *Coord. Chem. Rev.* **2016**, *307*, 211–236.

(42) Wang, Y.; Yang, J.; Li, Z.; Zhang, Z.; Li, J.; Yang, Q.; Zhong, C. Computational Study of

Oxygen Adsorption in Metal-Organic Frameworks with Exposed Cation Sites: Effect of Framework Metal Ions. *RSC Adv.* **2015**, *5*, 33432–33437.

(43) Parkes, M. V; Sava Gallis, D. F.; Greathouse, J. A.; Nenoff, T. M. Effect of Metal in M3(Btc)2 and M2(Dobdc) MOFs for O2/N2 Separations: A Combined Density Functional Theory and Experimental Study. *J. Phys. Chem. C* **2015**, *119*, 6556–6567.

(44) Sava Gallis, D. F.; Parkes, M. V; Greathouse, J. A.; Zhang, X.; Nenoff, T. M. Enhanced O2 Selectivity versus N2 by Partial Metal Substitution in Cu-BTC. *Chem. Mater.* **2015**, *27*, 2018–2025.

(45) Verma, P.; Maurice, R.; Truhlar, D. G. Identifying the Interactions That Allow Separation of O2 from N2 on the Open Iron Sites of Fe2(Dobdc). *J. Phys. Chem. C* **2015**, *119*, 28499–28511.

(46) Xiao, D. J.; Gonzalez, M. I.; Darago, L. E.; Vogiatzis, K. D.; Haldoupis, E.; Gagliardi, L.; Long, J. R. Selective, Tunable O2 Binding in Cobalt(II)–Triazolate/Pyrazolate Metal–Organic Frameworks. *J. Am. Chem. Soc.* **2016**, *138*, 7161–7170.

(47) Murray, L. J.; Dinca, M.; Yano, J.; Chavan, S.; Bordiga, S.; Brown, C. M.; Long, J. R. Highly-Selective and Reversible O2 Binding in Cr3(1,3,5-Benzenetricarboxylate)2. *J. Am. Chem. Soc.* **2010**, *132*, 7856–7857.

(48) Bae, Y.-S.; Spokoyny, A. M.; Farha, O. K.; Snurr, R. Q.; Hupp, J. T.; Mirkin, C. A. Separation of Gas Mixtures Using Co(Ii) Carborane-Based Porous Coordination Polymers. *Chem. Commun.* **2010**, *46*, 3478–3480.

(49) Bloch, E. D.; Queen, W. L.; Hudson, M. R.; Mason, J. A.; Xiao, D. J.; Murray, L. J.; Flacau, R.; Brown, C. M.; Long, J. R. Hydrogen Storage and Selective, Reversible O2 Adsorption in a Metal–Organic Framework with Open Chromium(II) Sites. *Angew. Chemie Int. Ed.* **2016**, *55*, 8605–8609.

(50) Xiao, D. J.; Gonzalez, M. I.; Darago, L. E.; Vogiatzis, K. D.; Haldoupis, E.; Gagliardi, L.; Long, J. R. Selective, Tunable O2 Binding in Cobalt(II)–Triazolate/Pyrazolate Metal–Organic Frameworks. *J. Am. Chem. Soc.* **2016**, *138*, 7161–7170.

(51) Li, Y.; Yang, R. T. Gas Adsorption and Storage in Metal−Organic Framework MOF-177. *Langmuir* **2007**, *23*, 12937–12944.

(52) Mu, B.; Schoenecker, P. M.; Walton, K. S. Gas Adsorption Study on Mesoporous Metal−Organic Framework UMCM-1. *J. Phys. Chem. C* **2010**, *114*, 6464–6471.

(53) Weston, M. H.; Farha, O. K.; Hauser, B. G.; Hupp, J. T.; Nguyen, S. T. Synthesis and Metalation of Catechol-Functionalized Porous Organic Polymers. *Chem. Mater.* **2012**, *24*, 1292–1296.

(54) Stoneburner, S. J.; Gagliardi, L. Air Separation by Catechol-Ligated Transition Metals: A Quantum Chemical Screening. *J. Phys. Chem. C* **2018**, *122*, 22345–22351.

(55) Yuan, S.; Feng, L.; Wang, K.; Pang, J.; Bosch, M.; Lollar, C.; Sun, Y.; Qin, J.; Yang, X.; Zhang, P.; et al. Stable Metal–Organic Frameworks: Design, Synthesis, and Applications. *Adv. Mater.* **2018**, *30*, 1704303.

(56) Howarth, A. J.; Liu, Y.; Li, P.; Li, Z.; Wang, T. C.; Hupp, J. T.; Farha, O. K. Chemical, Thermal and Mechanical Stabilities of Metal–Organic Frameworks. *Nat. Rev. Mater.* **2016**, *1*, 15018.

(57) Nguyen, H. G. T.; Weston, M. H.; Sarjeant, A. A.; Gardner, D. M.; An, Z.; Carmieli, R.; Wasielewski, M. R.; Farha, O. K.; Hupp, J. T.; Nguyen, S. T. Design, Synthesis, Characterization, and Catalytic Properties of a Large-Pore Metal-Organic Framework Possessing Single-Site Vanadyl(Monocatecholate) Moieties. *Cryst. Growth Des.* **2013**, *13*, 3528–3534.

(58) Fei, H.; Shin, J.; Meng, Y. S.; Adelhardt, M.; Sutter, J.; Meyer, K.; Cohen, S. M. Reusable Oxidation Catalysis Using Metal-Monocatecholato Species in a Robust Metal–Organic Framework. *J. Am. Chem. Soc.* **2014**, *136*, 4965–4973.

(59) Nguyen, H. G. T.; Mao, L.; Peters, A. W.; Audu, C. O.; Brown, Z. J.; Farha, O. K.; Hupp, J. T.; Nguyen, S. T. Comparative Study of Titanium-Functionalized UiO-66: Support Effect on the Oxidation of Cyclohexene Using Hydrogen Peroxide. *Catal. Sci. Technol.* **2015**, *5*, 4444–4451.

(60) Huang, Z.; Liu, D.; Camacho-Bunquin, J.; Zhang, G.; Yang, D.; López-Encarnación, J. M.; Xu, Y.; Ferrandon, M. S.; Niklas, J.; Poluektov, O. G.; et al. Supported Single-Site Ti(IV) on a Metal–Organic Framework for the Hydroboration of Carbonyl Compounds. *Organometallics* **2017**, *36*, 3921–3930.

(61) Zhang, X.; Vermeulen, N. A.; Huang, Z.; Cui, Y.; Liu, J.; Krzyaniak, M. D.; Li, Z.; Noh, H.; Wasielewski, M. R.; Delferro, M.; et al. Effect of Redox "Non-Innocent" Linker on the Catalytic Activity of Copper-Catecholate-Decorated Metal–Organic Frameworks. *ACS Appl. Mater. Interfaces* **2018**, *10*, 635–641.

(62) Weston, M. H.; Peterson, G. W.; Browe, M. A.; Jones, P.; Farha, O. K.; Hupp, J. T.; Nguyen, S. T. Removal of Airborne Toxic Chemicals by Porous Organic Polymers Containing Metal–Catecholates. *Chem. Commun.* **2013**, *49*, 2995–2997.

(63) Tanabe, K. K.; Siladke, N. A.; Broderick, E. M.; Kobayashi, T.; Goldston, J. F.; Weston, M. H.; Farha, O. K.; Hupp, J. T.; Pruski, M.; Mader, E. A.; et al. Stabilizing Unstable Species through Single-Site Isolation: A Catalytically Active TaV Trialkyl in a Porous Organic Polymer. *Chem. Sci.* **2013**, *4*, 2483–2489.

(64) Camacho-Bunquin, J.; Ferrandon, M.; Das, U.; Dogan, F.; Liu, C.; Larsen, C.; Platero-Prats, A. E.; Curtiss, L. A.; Hock, A. S.; Miller, J. T.; et al. Supported Aluminum Catalysts for Olefin Hydrogenation. *ACS Catal.* **2017**, *7*, 689–694.

(65) Wilmer, C. E.; Kim, K. C.; Snurr, R. Q. An Extended Charge Equilibration Method. *J. Phys. Chem. Lett.* **2012**, *3*, 2506–2511.

(66) Spek, A. L. Single-Crystal Structure Validation with the Program {\it PLATON}. *J. Appl. Crystallogr.* **2003**, *36*, 7–13.

(67) Spek, A. L. Structure Validation in Chemical Crystallography. *Acta Crystallogr. Sect. D* **2009**, *65*, 148–155.

(68) Willems, T. F.; Rycroft, C. H.; Kazi, M.; Meza, J. C.; Haranczyk, M. Algorithms and

Tools for High-Throughput Geometry-Based Analysis of Crystalline Porous Materials. *Microporous Mesoporous Mater.* **2012**, *149*, 134–141.

(69) Dubbeldam, D.; Calero, S.; Ellis, D. E.; Snurr, R. Q. RASPA: Molecular Simulation Software for Adsorption and Diffusion in Flexible Nanoporous Materials. *Mol. Simul.* **2016**, *42*, 81–101.

(70) Zhang, L.; Siepmann, J. I. Direct Calculation of Henry's Law Constants from Gibbs Ensemble Monte Carlo Simulations: Nitrogen, Oxygen, Carbon Dioxide and Methane in Ethanol. *Theor. Chem. Acc.* **2006**, *115*, 391–397.

(71) Witman, M.; Ling, S.; Jawahery, S.; Boyd, P. G.; Haranczyk, M.; Slater, B.; Smit, B. The Influence of Intrinsic Framework Flexibility on Adsorption in Nanoporous Materials. *J. Am. Chem. Soc.* **2017**, *139*, 5547–5557.

(72) Gee, J. A.; Sholl, D. S. Effect of Framework Flexibility on C8 Aromatic Adsorption at High Loadings in Metal–Organic Frameworks. *J. Phys. Chem. C* **2016**, *120*, 370–376.

(73) Wang, X.; Krishna, R.; Li, L.; Wang, B.; He, T.; Zhang, Y.-Z.; Li, J.-R.; Li, J. Guest-Dependent Pressure Induced Gate-Opening Effect Enables Effective Separation of Propene and Propane in a Flexible MOF. *Chem. Eng. J.* **2018**, *346*, 489–496.

(74) Bakhshian, S.; Sahimi, M. Theoretical Model and Numerical Simulation of Adsorption and Deformation in Flexible Metal–Organic Frameworks. *J. Phys. Chem. C* **2018**, *122*, 9465–9473.

(75) Moghadam, P. Z.; Fairen-Jimenez, D.; Snurr, R. Q. Efficient Identification of Hydrophobic MOFs: Application in the Capture of Toxic Industrial Chemicals. *J. Mater. Chem. A* **2016**, *4*, 529–536.

(76) Borycz, J.; Lin, L.-C.; Bloch, E. D.; Kim, J.; Dzubak, A. L.; Maurice, R.; Semrouni, D.; Lee, K.; Smit, B.; Gagliardi, L. CO2 Adsorption in Fe2(Dobdc): A Classical Force Field Parameterized from Quantum Mechanical Calculations. *J. Phys. Chem. C* **2014**, *118*, 12230–12240.

(77) Frenkel, D.; Smit, B. *Understanding Molecular Simulation: From Algorithms to Applications*; San Diego, CA: Academic Press, 2002.

(78) Dubbeldam, D.; Torres-Knoop, A.; Walton, K. S. On the Inner Workings of Monte Carlo Codes. *Mol. Simul.* **2013**, *39*, 1253–1292.

(79) Islamoglu, T.; Ray, D.; Li, P.; Majewski, M. B.; Akpinar, I.; Zhang, X.; Cramer, C. J.; Gagliardi, L.; Farha, O. K. From Transition Metals to Lanthanides to Actinides: Metal-Mediated Tuning of Electronic Properties of Isostructural Metal–Organic Frameworks. *Inorg. Chem.* **2018**, *57*, 13246–13251.

(80) Perdew, J. P.; Burke, K.; Ernzerhof, M. Generalized Gradient Approximation Made Simple. *Phys. Rev. Lett.* **1996**, *77*, 3865–3868.

(81) Grimme, S.; Antony, J.; Ehrlich, S.; Krieg, H. A Consistent and Accurate Ab Initio Parametrization of Density Functional Dispersion Correction (DFT-D) for the 94 Elements H-Pu. *J. Chem. Phys.* **2010**, *132*, 154104.

(82) Grimme, S.; Ehrlich, S.; Goerigk, L. Effect of the Damping Function in Dispersion Corrected Density Functional Theory. *J. Comput. Chem.* **2011**, *32*, 1456–1465.

(83) te Velde, G.; Bickelhaupt, F. M.; Baerends, E. J.; Fonseca Guerra, C.; van Gisbergen, S. J. A.; Snijders, J. G.; Ziegler, T. Chemistry with ADF. *J. Comput. Chem.* **2001**, *22*, 931–967.

(84) Fonseca Guerra, C.; Snijders, J. G.; te Velde, G.; Baerends, E. J. Towards an Order-N DFT Method. *Theor. Chem. Acc.* **1998**, *99*, 391–403.

(85) Baerends, E. J.; Ziegler, T.; Atkins, A. J.; Autschbach, J.; Bashford, D.; Baseggio, O.; Bérces, A.; Bickelhaupt, F. M.; Bo, C.; Boerritger, P. M.; et al. ADF2017, SCM, Theoretical Chemistry, Vrije Universiteit, Amsterdam, The Netherlands, https://www.scm.com.

(86) Van Lenthe, E.; Baerends, E. J. Optimized Slater-Type Basis Sets for the Elements 1–118. *J. Comput. Chem.* **2003**, *24*, 1142–1156.

(87) Lenthe, E. van; Baerends, E. J.; Snijders, J. G. Relativistic Regular Two-component Hamiltonians. *J. Chem. Phys.* **1993**, *99*, 4597–4610.

(88) van Lenthe, E.; Baerends, E. J.; Snijders, J. G. Relativistic Total Energy Using Regular Approximations. *J. Chem. Phys.* **1994**, *101*, 9783–9792.

(89) van Lenthe, E.; Ehlers, A.; Baerends, E.-J. Geometry Optimizations in the Zero Order Regular Approximation for Relativistic Effects. *J. Chem. Phys.* **1999**, *110*, 8943–8953.

(90) Kresse, G.; Furthmüller, J. Efficient Iterative Schemes for Ab Initio Total-Energy Calculations Using a Plane-Wave Basis Set. *Phys. Rev. B* **1996**, *54*, 11169–11186.

(91) Blöchl, P. E. Projector Augmented-Wave Method. *Phys. Rev. B* **1994**, *50*, 17953–17979.

(92) Yang, D.; Momeni, M. R.; Demir, H.; Pahls, D. R.; Rimoldi, M.; Wang, T. C.; Farha, O. K.; Hupp, J. T.; Cramer, C. J.; Gates, B. C.; et al. Tuning the Properties of Metal-Organic Framework Nodes as Supports of Single-Site Iridium Catalysts: Node Modification by Atomic Layer Deposition of Aluminium. *Faraday Discuss.* **2017**, *201*, 195–206.

(93) Planas, N.; Mondloch, J. E.; Tussupbayev, S.; Borycz, J.; Gagliardi, L.; Hupp, J. T.; Farha, O. K.; Cramer, C. J. Defining the Proton Topology of the Zr6-Based Metal–Organic Framework NU-1000. *J. Phys. Chem. Lett.* **2014**, *5*, 3716–3723.

(94) Tang, W.; Sanville, E.; Henkelman, G. A Grid-Based Bader Analysis Algorithm without Lattice Bias. *J. Phys. Condens. Matter* **2009**, *21*, 84204.

(95) Sanville, E.; Kenny, S. D.; Smith, R.; Henkelman, G. Improved Grid-Based Algorithm for Bader Charge Allocation. *J. Comput. Chem.* **2007**, *28*, 899–908.

(96) Henkelman, G.; Arnaldsson, A.; Jónsson, H. A Fast and Robust Algorithm for Bader Decomposition of Charge Density. *Comput. Mater. Sci.* **2006**, *36*, 354–360.

(97) Yu, M.; Trinkle, D. R. Accurate and Efficient Algorithm for Bader Charge Integration. *J. Chem. Phys.* **2011**, *134*, 64111.

(98) Bader, R. F. W. *Atoms in Molecules: A Quantum Theory*; Oxford University Press: New

York, 1990.

TOC Graphic

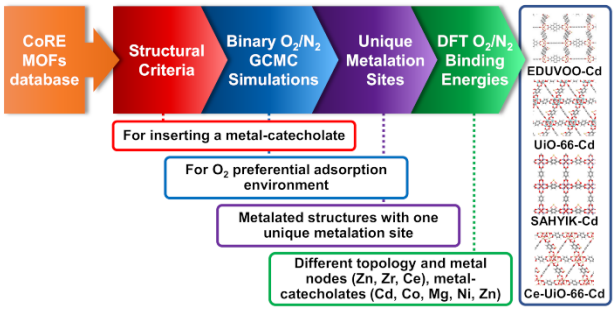
CoRE MOFs database
Structural Criteria
Binary O_2/N_2 GCMC Simulations
Unique Metalation Sites
DFT O_2/N_2 Binding Energies
EDUVOO-Cd
UiO-66-Cd
SAHYIK-Cd
Ce-UiO-66-Cd
For inserting a metal-catecholate
For O_2 preferential adsorption environment
Metalated structures with one unique metalation site
Different topology and metal nodes (Zn, Zr, Ce), metal-catecholates (Cd, Co, Mg, Ni, Zn)